## PAPER

# Direct 2D measurement of time-averaged forces and pressure amplitudes in acoustophoretic devices using optical trapping

Stefan Lakämper,†‡[a] Andreas Lamprecht,†‡*[a] Iwan A. T. Schaap‡[bc] and Jurg Dual‡[a]

Ultrasonic standing waves are increasingly applied in the manipulation and sorting of micrometer-sized particles in microfluidic cells. To optimize the performance of such devices, it is essential to know the exact forces that the particles experience in the acoustic wave. Although much progress has been made *via* analytical and numerical modeling, the reliability of these methods relies strongly on the assumptions used, *e.g.* the boundary conditions. Here, we have combined an acoustic flow cell with an optical laser trap to directly measure the force on a single spherical particle in two dimensions. While performing ultrasonic frequency scans, we measured the time-averaged forces on single particles that were moved with the laser trap through the microfluidic cell. The cell including piezoelectric transducers was modeled with finite element methods. We found that the experimentally obtained forces and the derived pressure fields confirm the predictions from theory and modeling. This novel approach can now be readily expanded to other particle, chamber, and fluid regimes and opens up the possibility of studying the effects of the presence of boundaries, acoustic streaming, and non-linear fluids.

## Introduction

The arrangement of small objects with ultrasonic waves (US) finds widespread use in diverse fields such as chemistry, material sciences and medicine. The efficient spatial manipulation with US of hard spherical objects within a microfluidic device, the fluid being either stationary or flowing,[1,2] is of high interest for small-scale biomedical devices due to its non-contact nature and its comparatively low-cost implementation. Examples include the generation of transport for controlled mixing.[3] Also, biological cells with different acoustic properties can be sorted by acoustic forces.[4,5]

To optimize the development of ultrasonically modulated microfluidic cells, it is important to understand which forces the particles experience in a certain design. While theories have been developed and several applications have been shown, concomitant complications regarding geometry, fluid

[a] *Department of Mechanical and Process Engineering, Institute of Mechanical Systems, ETH, Zürich, Switzerland. E-mail: lamprecht@imes.mavt.ethz.ch*
[b] *Drittes Physikalisches Institut, Georg-August Universität, Göttingen, Germany*
[c] *Center for Nanoscale Microscopy and Molecular Physiology of the Brain (CNMPB), Göttingen, Germany*
† These authors contributed equally to this work.
‡ The experiment was conceived by SL; the optical trapping apparatus was designed by IATS. SL and AL modified the apparatus for large-scale position recordings, developed the adapted ultrasonic measurement chamber and performed all experiments and data analysis. The manuscript text and figures were prepared by SL and AL with feedback from JD and IATS.

properties and material properties made the reproducible determination of fundamental parameters like pressure amplitude or force in a dedicated measurement system difficult.[6] Acoustic streaming phenomena make these issues even more complicated.

For the performance of lab on a chip (LOC) devices, the acoustic energy related to the squared pressure is the decisive parameter; that is why it needs to be measured.[22] In the research field of device development, the acoustic pressure distribution is of essential interest to reach the targeted functions of the device. So far, COMSOL simulations provided the information about the pressure distribution, and by experimental qualitative observations, the numerical results were proven. These observations do not provide a quantitative validation of the simulation and the real acoustic pressure amplitudes remain unknown. Our direct force measurements are therefore highly relevant and close the gap of missing information about the acoustic pressure distribution inside a LOC device.

Recently, three experimental approaches have been used to measure the total time-averaged acoustic force on particles in ultrasonic devices. In a systematic series of publications by Barnkob *et al.*,[7] microparticle image velocimetry (μPIV) was used to infer the force on moving particles in an acoustic field in 2D. In the 2D paper, the focus was on measuring the forces, while in the 3D paper the streaming patterns were investigated.[29] Also, the intrinsically 2D observations of the bead motion make the analysis of motions in the 3rd dimension

difficult. Nevertheless, as calculated from the velocity of a bead moving against the surrounding fluid drag (Stokes drag), the authors find good agreement between theoretical descriptions and experimental data. The advantage of using an optical trap is that it has higher time resolution and it directly measures the force at a particular location. Because the time constant of generating the streaming is different from the time constant of generating the acoustic radiation force, this might actually allow the separation of the two effects in the future. Thalhammer et al.[8] estimated the force by the indirect use of an optical trapping system[9,10] which was combined with a capillary device: a long-range optical trap with a modulated beam profile was used to generate an optical trap with a long working distance. By using a mirrored piezo-acoustic transducer, the counter-propagating optical trap was formed perpendicular to the plane generated by the acoustic field. Acoustical excitation confined the objects in a plane. Beads were first displaced from that plane by use of the optical trap and then let go by switching off the optical trap. The bead motion was monitored in 1D by video imaging from the side of the square section of the capillary. This intricate measurement setup allowed for qualitatively observing the displacement of a large polystyrene bead that was optically held with respect to the driving frequency of the actuator. Independent determination of the trap stiffness using other particles was used to infer the force acting on this particle.

In a second experimental approach, Thalhammer et al. used the same optical trap setup as a positioning device in order to first locate the trapped bead at a position far from the nodal plane generated by the acoustic field. After switching off the optical trap, the position and velocity of the particle moving towards the nodal plane of the acoustic potential were monitored. Again, the drag force was used to infer the acoustic forces. The results show a good correlation between the theory and the obtained experimental data. Recently, holographic optical tweezers were used to measure 2D forces in an acoustic standing wave that was generated at a fixed frequency in a special device and compared to PIV measurements.[11]

The aforementioned experiments show that in principle it is possible to measure the forces acting on the particles that are manipulated with US. However, the spatial constraints of the used techniques make it difficult to test the more challenging scenarios that can occur in the usual microfluidic cells. We therefore set out to design a combined optical and acoustical trap that exploits all advantages of using a single beam optical trap,[12] featuring an objective with a high numerical aperture and an in situ trap calibration (see Fig. 1a and b) in at least two dimensions. To accommodate the optical trap in the combined instrument, we designed a transparent acoustophoretic device with a side-mounted actuator (see Fig. 1b). In this report, we provide measurements which quantify the total acoustic forces on beads of different
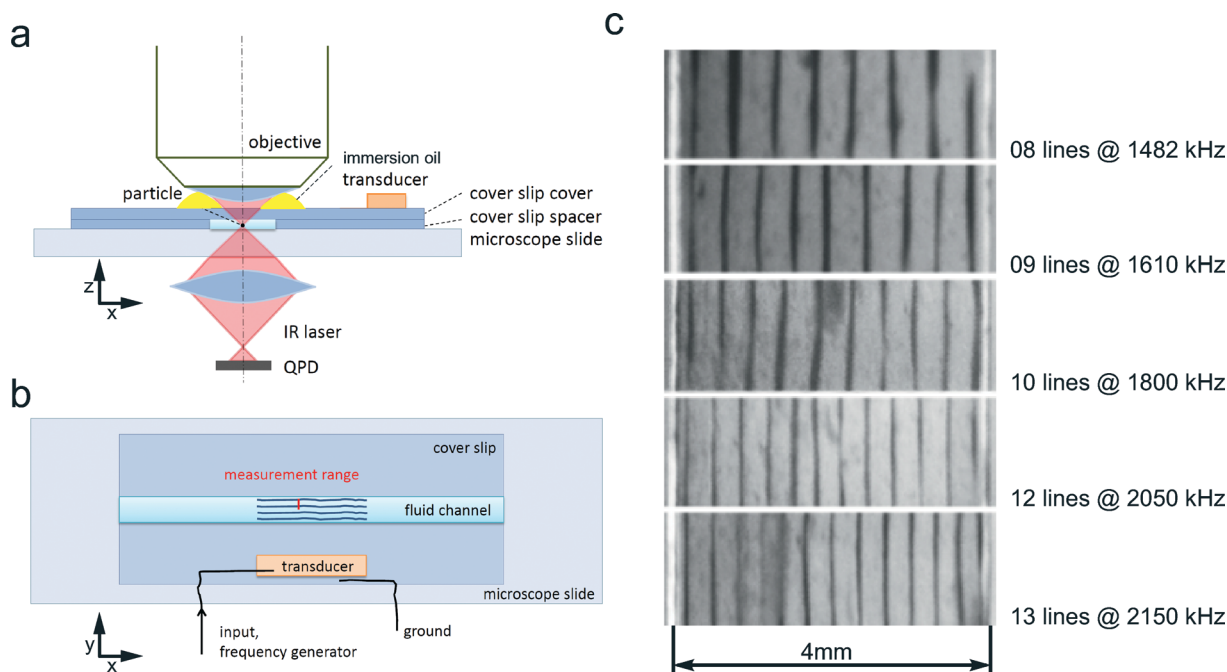


Fig. 1  Acoustic flow cell, design and performance: a.) and b.) show schematic illustrations of the acoustic device (side view in a) and top view in b)) and the simplified main optical components in a). A standard microscope slide carries two spacers cut from a coverslip to form a 4 mm wide channel that is covered with another coverslip. Glued together by epoxy, the device carries a piezoelectric transducer of about 8 mm × 2 mm × 1 mm size, in parallel to the channel length (x) but offset by about 8 mm to accommodate the high numerical aperture objective needed for optical trapping and position detection. The laser trap allows one to hold and manipulate individual beads and is formed by a tightly focused laser beam of 980 nm wavelength. After the trap, the laser light is collected and projected on a quadrant photodetector. c.) shows bulk experiments using a large amount of 7.61 μm diameter silica beads which form the indicated number of parallel lines at the indicated acoustic driving frequency (see also Fig. 3c). The experiments were done with an excitation amplitude of 5 V.

diameters in US of different frequencies in 2D. We found a good agreement with theory and we will discuss the potential of this novel approach.

## Materials and methods

### Optical trapping setup

The optical trapping apparatus (Fig. 1a) is a simplified setup of the one that we described in detail elsewhere.[13] Briefly, a collimated 330 mW, 980 nm laser beam (unless mentioned, all opto-mechanical components were obtained from Thorlabs, Dachau, Germany) with variable power is coupled to the optical path of a standard microscope chassis (Olympus CH, Tokyo, Japan). To form the optical trap, the laser beam is tightly focused in the flow cell by a high-numerical aperture objective (Neofluar 100× 1.3 NA, Zeiss, Germany). The position of a trapped particle is monitored by the transmitted laser light, which, after collection by an air condenser (Olympus, Tokyo, Japan), is cast on a quadrant photodetector (QPD). The analog difference signals that encode the bead position are digitized (NI USB-6212, National Instruments, Austin, TX, US) and analyzed using a custom-written LabVIEW routine.

The trap stiffness $\kappa$ and the detector response were calibrated by recording the power spectrum of the position signal of the trapped bead and applying the equipartition theorem.[14] The thermal motion of the trapped particle is detected by the QPD and transformed into a Lorentzian power spectrum. Fig. 2 shows the power spectrum (black) of a 4.39 μm particle in water at 20 °C for several laser powers. The linear optical trapping stiffness $\kappa$ for small particle displacements (<particle radius $r_s$) in the plane orthogonal to the beam direction is:[15]

$$k = 2\pi\gamma f_c \qquad (1)$$

where $f_c$ is the 3dB cutoff frequency of the Lorentzian power spectrum and $\gamma$ is the Stokes drag term defined as $\gamma = 6\pi\mu r_s$ with $\mu$ as the dynamic fluid viscosity.

### Ultrasonic device

The ultrasonic measurement device (Fig. 1b) needed to fulfill several geometric requirements, which required a different design compared to our earlier devices. The device needed to be easy to assemble and reusable, to show minimal acoustic streaming and to be adapted to the optical trapping setup, *i.e.* translucent and with the piezoelectric actuator mounted outside of the optical path. Solid-state machined, wafer-based PDMS devices proved to be too small to accommodate the objective lens of the trapping setup. Furthermore, in such devices, the actuators are often mounted on the bottom side and the optical properties of the used materials are incompatible with the optical trap. Therefore, we constructed our devices from standard microscope slides and cover slips (MENZEL GmbH, Menzel-Gläser, Braunschweig, Germany). The material has defined standard sizes, has standardized optical properties and is easily cut with a wafer saw to provide geometrically accurate positioning of the channel walls in the spacer layer. #00 (thickness 55–80 μm) microscope coverslips were used for both spacer and cover. We tested several methods to efficiently connect the three layers forming the channel and found that polyurethane spray glue provided the best results (ITW, Cramolin Urethan, Mühlacker, Germany). A standard-size piezo-acoustic actuator (Ferroperm, Pz26, $l \times w \times h$ = 8 mm × 2 mm × 1 mm, Kvistgaard, Denmark), which has its first thickness eigenfrequency at 1950 kHz including contact wiring, was glued on the cover layer using conductive glue (EPOXY Technology, H20E, Billerica, MA, USA). Acoustic coupling into the channel proved to be much more efficient and reproducible in this full glass device as compared to other composite devices made of combinations of other materials, like PDMS. In order to accommodate the objective lens and to have the ability to move the trap along the whole width of the channel, the ultrasonic actuator was positioned at about 8 mm distance from the channel. In the process of device development, we optimized the efficiency of coupling by shifting the actuator in steps of 1 mm over a range from 3 to 10 mm distance. At a position of 8 mm, the line forming capacity of the device was found optimal when using bulk suspensions of silica beads.

### Data acquisition

For single particle measurements, the device was filled with a dilute bead suspension in distilled water. A single particle (7.61 μm, 6.55 μm or 4.39 μm diameter monodisperse research silica, Microparticles GmbH, Berlin, Germany) was trapped at high laser power (75 to 250 mW) and positioned in the middle between the lower and the upper boundary of the channel (which corresponded to approximately 30–40 μm
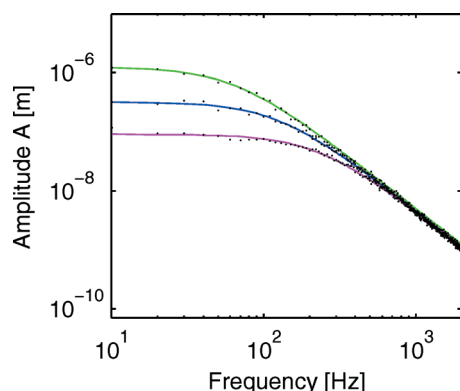


**Fig. 2** The power spectrum of bead motion at three different laser powers is shown with their specific fitted curves: 75 mW (GREEN), 150 mW (BLUE), and 250 mW (MAGENTA). The fit of the experimental detected transfer function of the thermal bead motion within the optical trap was done as described by Svoboda *et al*. These experiments were done with 4.39 μm diameter silica particles in water. Their corresponding 3dB cutoff frequencies $f_c$ are located at 41.99 Hz, 73.98 Hz and 145.97 Hz and can be used to calculate the optical trap stiffness by eqn (1) as 0.021 pN nm⁻¹, 0.039 pN nm⁻¹ and 0.076 pN nm⁻¹, respectively.

distance from the top and bottom, respectively). This avoids a.) corrections for the increased drag due to the vicinity of a surface (Faxen's law, see also ref. 16) and b.) possible effects caused by acoustic streaming or c.) large optical distortion by particles sticking to the top or bottom layer. As the total measurement time required about 3–5 hours, the evaporation of the suspension was counteracted by two water-filled reservoirs at each channel opening. Liquid flow due to unequal filling levels could be observed by particles flowing by. Flow was stopped either by leveling or by letting the system equilibrate. After trapping a single particle and positioning it at appropriate and standardized distances, the stiffness of the optical trap was determined several times using the custom-written power spectral density method at 75-250 mW laser power. Intermittent determination of the trap stiffness during an ongoing measurement set confirmed that the trap stiffness did not change significantly over the course of the measurement. The acoustic experimental setup uses a frequency generator (Tektronix, AFG 3022B, Beaverton, OR, USA), which drove the input of a power amplifier (MKS Instrumente Deutschland GmbH, ENI 2100L RF, Bernhausen, Germany). The amplified sinusoidal excitation signal is connected to the piezoelectric transducer on the device and defines the acoustic excitation by its frequency and amplitude. For a whole set of data, we performed a series of up to 40 frequency sweeps, ranging from 1100–2300 kHz within 240 s (5 kHz s$^{-1}$), at 30–50 μm intervals along the $y$ axis of the channel (red line in Fig. 1b). A linear encoder (Numerik Jena GmbH, LIK 41-M12-TZ, Jena, Germany) was used to record the position of the stage. The time constant of the particle dynamics is dominated by the viscous drag forces (Stokes Law) and it was ensured that this time constant is much smaller than the frequency increase rate of 5 ms per 1 Hz to avoid any delay in the observed particle displacement.

The corresponding viscous time constant $T_{Drag} = \dfrac{m_s}{\gamma}$ is 6.43 μs for a 7.61 μm diameter silica particle in water, where $m_s$ is the particle mass. For each sweep, we recorded a video of the bead motion. To synchronize the recording with the frequency sweeps, the linear frequency scan was interrupted at equal intervals by pausing the excitation. This provided complete and reliable referencing in our reduced and non-automated measurement system.

### Data analysis

In order to determine the displacement and behavior of the trapped bead during a frequency scan, we analyzed the video sequences using a particle tracking routine (X Citex Inc., ProAnalyst, Particle Tracking Tool, Cambridge, MA, USA). Because the software did not pick the same virtual reference for the different videos, we defined the zero displacement position for each single measurement by subtracting the mean value of the sinusoidal displacement/force curves.

Within the combined potential of the optical trap and the overlaid acoustical excitation, the video-based data acquisition

at 30 fps is appropriate, as the relevant time constants from an acoustical, optical and fluid dynamical perspective are much smaller. The information was correlated off-line with the excitation pattern to determine the start, end and zero excitation position of the particle. Subsequent analysis for the determination of the average displacement in the $x$- and $y$-directions for a given frequency and all conversions to force (using $\kappa$), eigenfrequency, pressure amplitude and response were performed using a custom-written MatLab code.

### Modeling

We performed finite element simulations to evaluate the results by modelling the resonant cavity and the surrounding mechanical structure. To reduce the computing time, we simulated the experimental device in 2D using COMSOL Multiphysics version 4.2a (COMSOL Inc., Burlington, MA, USA). The geometry built in the finite element model is shown in Fig. 1a, the dimensions of the fluid chamber are $h \times w$ = 0.06 mm × 4 mm (Fig. 1b). The following material properties have been used: water density $\rho$ of 998 kg m$^{-3}$, a corresponding speed of sound of $1481(1 + i/(2 \times 246.3))$ m s$^{-1}$ (a value including damping effects, own unpublished work by P. Hahn), Young's modulus (glass) of $63(1 + i/400)$ GPa, a Poisson ratio $v$ of 0.2, and a density of 2220 kg m$^{-3}$. The piezoelectric element (Ferroperm, Pz26, Kvistgaard, Denmark) was "defined" according to the producer's specifications.

The viscous damping of the fluid was realized by the complex wave speed and the energy loss of solid materials was considered by complex stiffness parameters. Viscous damping within the fluid cavity is a dominating effect here because of the narrow channel height of 55–80 μm.

The water domain was modeled by the use of the pressure acoustic physics module of COMSOL. The dependent variable is the acoustic pressure $p$. All cavity boundaries are excited by normal acceleration. This coupling is part of the solid mechanics physics module (solid) of COMSOL, in which glass is represented as an isotropic material. There, the dependent variable is the displacement field $v$. All outside boundaries are free in their displacement and the boundary condition for the fluid boundary interaction was defined as the boundary load from the pressure acoustic physics module. This load is related to the acoustic pressure and couples the waves back into the device structure.

The meshing was done by using "auto mesh" with the condition that the allowed minimum size of the largest element is four times smaller than the lowest wavelength during the simulation. The calculations of COMSOL were done in the frequency domain by the use of the PARADISO solver. The solver configuration "fully coupled" was applied such that the coupling between the solid mechanics physics and the pressure acoustic physics module was assured. The parametric simulation was done over a frequency range from 1200 to 2400 kHz in 2 kHz steps.

Because the reduction to a 2D simulation yields a slightly stiffer system, the first three simulated eigenmodes are higher than the ones experimentally determined (Fig. 4b).

## Forces on particles

Acoustic radiation forces control the motion of the particles within an acoustic manipulation device if acoustic streaming can be neglected.

First calculations of acoustic forces due to an incident plane wave for incompressible particles in a non-viscous fluid were done by King.[17] Yosioka *et al.*[18] expanded King's theory to compressible particles for one-dimensional forces. The time-averaged acoustic force $F$ with its amplitude $A_F$ was derived as

$$F = \frac{\omega}{2\pi}\int_0^{\frac{2\pi}{\omega}} F\mathrm{d}t = A_F \sin(2k_p y_s) \qquad (2)$$

where

$$A_F = \frac{\pi}{\rho_f \omega^2} A_P^2 \left(k_p r_s\right)^3 \Phi \qquad (3)$$

The index "$f$" corresponds to the fluid and "$s$" to the particle specific properties and $k_p = \dfrac{2\pi}{\lambda_p}$ is the wave number of the acoustic pressure field, where $\omega$ is the angular frequency of the excitation, $\rho$ is the density, and $y_s$ is the particle position within the acoustic pressure field with its amplitude $A_P$. In eqn (2), it can be seen that the wavelength $\lambda_F$ of the force field is by a factor of 2 smaller than the wavelength $\lambda_P$ of the pressure field, an illustration is shown in Fig. 4. The acoustic contrast factor $\Phi$ was defined by Yosioka[18] as

$$\Phi = \frac{f_1}{3} + \frac{f_2}{2} \qquad (4)$$

where the compressibility factor $f_1$ and the density factor $f_2$, are given as

$$f_1 = 1 - \frac{\rho_f c_f^2}{\rho_s c_s^2} \text{ and } f_2 = \frac{2(\rho_s - \rho_f)}{2\rho_s + \rho_f}, \qquad (5)$$

where $c$ is the speed of sound. Depending on $\Phi$, particles accumulate either at locations corresponding to the pressure nodes ($\Phi > 0$) or the velocity nodes ($\Phi < 0$), which, relative to each other, are shifted by $\dfrac{\lambda}{4}$ in the direction of the wave propagation. For the most commonly used particles and biological cells, the pressure nodes will correspond to the equilibrium position. Fig. 4a schematically illustrates the acoustic pressure and velocity field and the resulting equilibrium positions of small spherical particles with $\Phi > 0$.

An expanded and more general method to calculate the time-averaged acoustic force in all three dimensions is Gor'kov's theory:[19] he defined the acoustic radiation force $F$ as a gradient force of the potential $U$, with

$$\boldsymbol{F} = -\nabla U \qquad (6)$$

and

$$U = 2\pi r_s^3 \rho_f \left( \frac{1}{3}\frac{\langle p^2 \rangle}{\rho_f^2 c_f^2} f_1 - \frac{1}{2}\langle |\boldsymbol{u}|^2 \rangle f_2 \right), \qquad (7)$$

where $|\boldsymbol{u}|^2 = \boldsymbol{u}_x^2 + \boldsymbol{u}_y^2 + \boldsymbol{u}_z^2$.

The variables indicated with $<..>$ are their time-averaged values over one wave cycle. The representation of Gor'kov shows that the particles will move to the minima of the force potential $U$ within the acoustic field. The positions of these minima in the acoustic field are dependent on the compressibility factor $f_1$ and the density factor $f_2$. For the one-dimensional case, Yosioka's and Gor'kov's results are the same.

Additionally, the particle experiences balancing viscous forces, *i.e.* Stokes drag, as the particle starts to move in a viscous medium. Furthermore, depending on the boundary conditions, the acoustic excitation can generate streaming effects which can influence the particle behavior. These can be either local streaming in the vicinity of the particle[20] or streaming determined by the device geometry, causing fluid flow within the chamber.[21]

## Experimental results and discussion

### Interferometry measurements

In a linear acoustic system, the excitation amplitude and the acoustic pressure amplitude are directly proportional; eqn (2) yields a quadratic relation between the pressure amplitude and the acoustic force (Fig. 4c).

The linear dependency between the frequency generator output (10–150 mVpp) and the displacement signal of the piezoactuator itself was independently checked (data not shown). For this, experiments were done with a laser interferometer (Polytech GmbH, OFV-505, Waldbronn, Germany) in combination with a signal controller (Polytech GmbH, DFV-500, Waldbronn, Germany). The laser measurement point was chosen on a defined point on the upper transducer surface and the controller output was detected with an oscilloscope (Teledyne LeCroy, Wavesurver 424, New York, NY, USA).

### Eigenfrequencies

According to the 1D theoretical formulation, the acoustic force on a particle has to behave in a sinusoidal manner relative to the equilibrium position (eqn (2)). When an optically trapped particle is held away from an equilibrium position, the particle will experience an acoustic force which will push the particle out of the trap. To quantify the acoustic force, we measured the displacement response of a single trapped particle of defined diameter with respect to a linear continuous frequency sweep from 1400 to 2300 kHz in 240 s. This measurement was repeatedly performed at intervals of 30 μm

over a full distance of 1110 μm in the $y$-direction in the US device (Fig. 1b, red line). Each resulting measurement set (Fig. 3a) was first analyzed with respect to the determined modes (eigenfrequencies) by its sinusoidal form. An alternating pattern of positive and negative displacements in the $y$-direction can be observed already roughly by the eye (see Fig. 3a). The optimum frequencies were determined analytically using a MatLab code, which compares the different plots of raw data along the $y$-axis for each frequency. The best plot to fulfill the conditions of a sinusoidally shaped eigenmode was chosen.

The force field wavelength of an $n$-line mode in a micromanipulation device with sound-hard boundaries should be $\lambda_n = \dfrac{b}{n}$.[22,23] In Fig. 3d, we compared the results obtained by
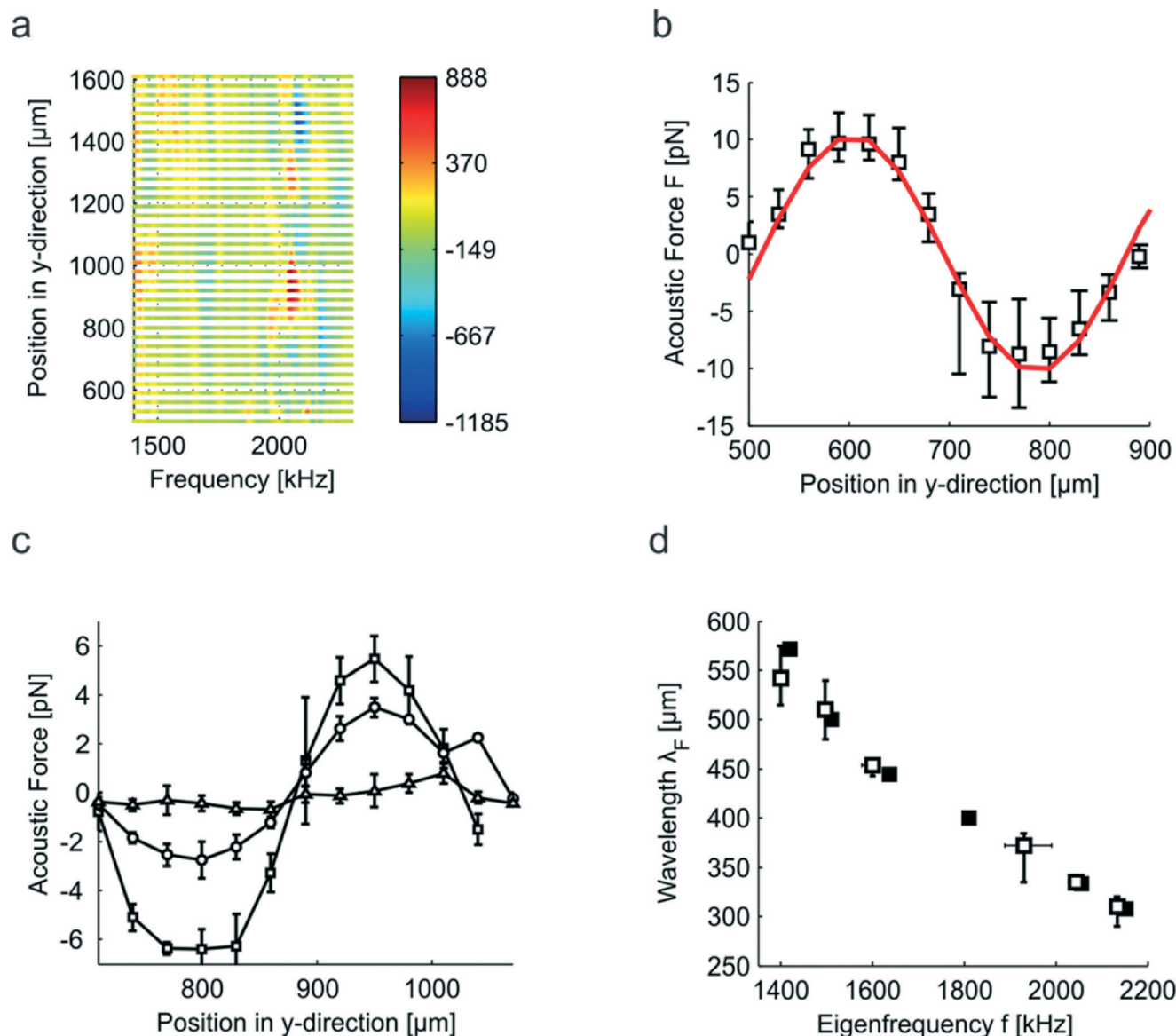


Fig. 3 Acoustic forces on optically trapped beads. a.) Raw data obtained from frequency scans at 30 μm intervals in the $y$-direction. The absolute distance is given as the distance to the sidewalls of the spacing cover slide. The false color scheme represents the observed displacement in nm at a given position and a given frequency, red being positive and blue being negative with respect to the absolute $y$-position. b.) The force as calculated from the bead displacement and the trap stiffness in relation to the $y$-position for a frequency of 2044 kHz. Three different data sets from independent measurements using 7.61 μm silica particles are shown as average values with absolute error. The different curves were aligned along the horizontal axis to compensate for small differences between the different experiments (temperature, positional readout accuracy). The solid RED line shows the sinusoidal fitting curve of the measurements. c.) The acoustic force increases with the particle volume at a given frequency $f =$ 2044 kHz and a given material without changing the wavelength of the position signal: here, three independent measurements of particles of different sizes are compared; squares, circles and triangles indicate particle diameters of 7.61, 6.55 and 4.39 μm, respectively. d.) The force wavelengths $\lambda_F$ observed for different particle sizes at a given frequency and wavelength are averaged (open squares) and the absolute data spans are indicated as error bars. These data are compared with the data from COMSOL simulations (solid squares).

COMSOL Multiphysics with the modes and wavelengths determined experimentally using our laser trapping apparatus. Error bars in Fig. 3d show the absolute span of the averaged values at a given excitation frequency. With this and the number of lines observed over the span of the chamber, it is possible to assign the theoretical modes to the observed particle lines in the experiments. Because the reduction to a 2D simulation yields a slightly stiffer system, the first simulated eigenmodes have higher wavelength than the ones experimentally determined (Fig. 3d).

Interestingly, in the numerical 2D simulations, the 11-line mode (1920 kHz) showed an extremely weak signal, coinciding with the weak line formed in the bulk experiment (Fig. 1c, 1920 kHz). From the optical trap experiments, the weakest signal in the full set of experiments was obtained in the 10-line mode (Fig. 3a), where the bulk experiments showed good line forming (Fig. 1c), the reason for this is unclear at the moment. However, the eigenfrequencies in simulations and experiment coincide exquisitely well, indicating that we obtain physically meaningful information from a "pure" and stable linear acoustic system.

## Converting displacement signals to averaged acoustic forces on the particle

The displacements along the $y$-direction at a specific eigenfrequency can be readily converted to forces: the optical trap stiffness is linear for small displacements.[9,16,24] This allows one to directly scale the displacement curves with the measured trap stiffness. Therefore, we first performed measurements using particles with the same size to predict the reliability of the acoustic force prediction with the experimental setup. For our analysis, the measured force curves have to be overlapped. This procedure requires post-process manual alignment of the curves along the $y$-axis. During measurement, the experimental environment (*e.g.* temperature) might change slightly and subsequently affect the wave propagation. Therefore, the pressure nodes of the plane standing wave showed a small difference in the $y$-direction between individual measurements. This offset was corrected in the force comparison. The averaged experimental results for a frequency of 2044 kHz are shown in Fig. 3b. The red bold curve is the sinusoidal fitting curve to the mean values of the measurements. This averaged acoustic force curve formed the basis for acoustic pressure calculations.

Fundamentally, the acoustic force is proportional to the particle volume.[19] Fig. 3c therefore shows the forces exerted on particles of different diameters between 7.61 and 4.39 μm at 2044 kHz. The force amplitudes show the expected dependency on the particle volume.

## Acoustic pressure prediction

The wavelength $\lambda_F$ of the averaged acoustic force curve is half the wavelength $\lambda_P$ of the acoustic pressure and is illustrated in Fig. 4a. Yosioka's theory of eqn (2) gives the relation between the acoustic force amplitude $A_F$ and the acoustic pressure amplitude $A_P$. Here, the pressure amplitude $A_P$ is the only unknown parameter because the particle position $y_s$ is defined by the position of the optical trap within the fluid chamber as well as the wave number $k_F$ of the acoustic force. Under the assumption that this relation holds for each single point of the averaged acoustic force curve, it is straightforward to calculate the acoustic pressure for $\lambda_P = 2\lambda_F$. Subsequent averaging of the calculated pressure amplitudes leads to an acoustic pressure distribution of the investigated measurement range along the $y$-direction for a particular eigenmode. The individual force amplitudes can vary with respect to the averaged force amplitude by ±50% for one specific eigenmode. Experimental data for this variation can be seen in Table 1. These differences are probably caused by slight disturbances in the acoustic boundary conditions or temperature during the measurement.

Since the measurement of the acoustic pressure is independent of the particle size trapped in the laser focus, measurements of particles of three different diameters (7.61 μm, 6.55 μm and 4.39 μm) were taken into account. The average and absolute span of the determined acoustic pressure amplitudes of all measurements are shown in Fig. 4b in comparison with the COMSOL data, which confirms that the particle size has no obvious influence on the determined amplitudes (open squares). The numerically determined pressure amplitudes (solid squares) correspond very well to the experimental results. In all graphs, error bars indicate the absolute span of data rather than statistical errors, thus giving complete and unbiased information.

To confirm that the particle size has no effect on the acoustic pressure, we also calculated the pressure amplitude for the three particles of different sizes shown in comparison with respect to the force in Fig. 3c. The data for the different sizes was recorded at the same excitation frequency and eigenmode, and taken at the same absolute position within the device (as seen on the $x$-axis in Fig. 3c), showing the theoretical behaviour with respect to the relation of size and force. Taking these three individual data sets for the calculation of the actual pressure amplitude, we obtain values that differ by ±10%, as shown in Table 3. Due to the above stated selection criteria, the $|A_{F\,max}|$ in Table 3 differs from the data given in Table 1, which shows that the measurements of the pressure amplitude are completely independent of the particle size.

In the context of the determination of the actual pressure amplitude at a given resonant frequency, we double-checked the effect of the offset of the sinusoidal force signals with respect to the $y$-position: to remind us, at a given frequency, we determine the displacement with respect to the trap center along the $y$-axis. The resulting values of $F$ show a sinusoidal behavior with robust correlation to the globally determined and calculated mode number, but show a positive or negative offset in $F$. For the actual calculation of the pressure amplitude, we calculated both the averages of individual $|A_F - A_{F\,mean}|$ and subsequently the resulting pressure amplitude $A_P$. To double-check, we calculated the individual
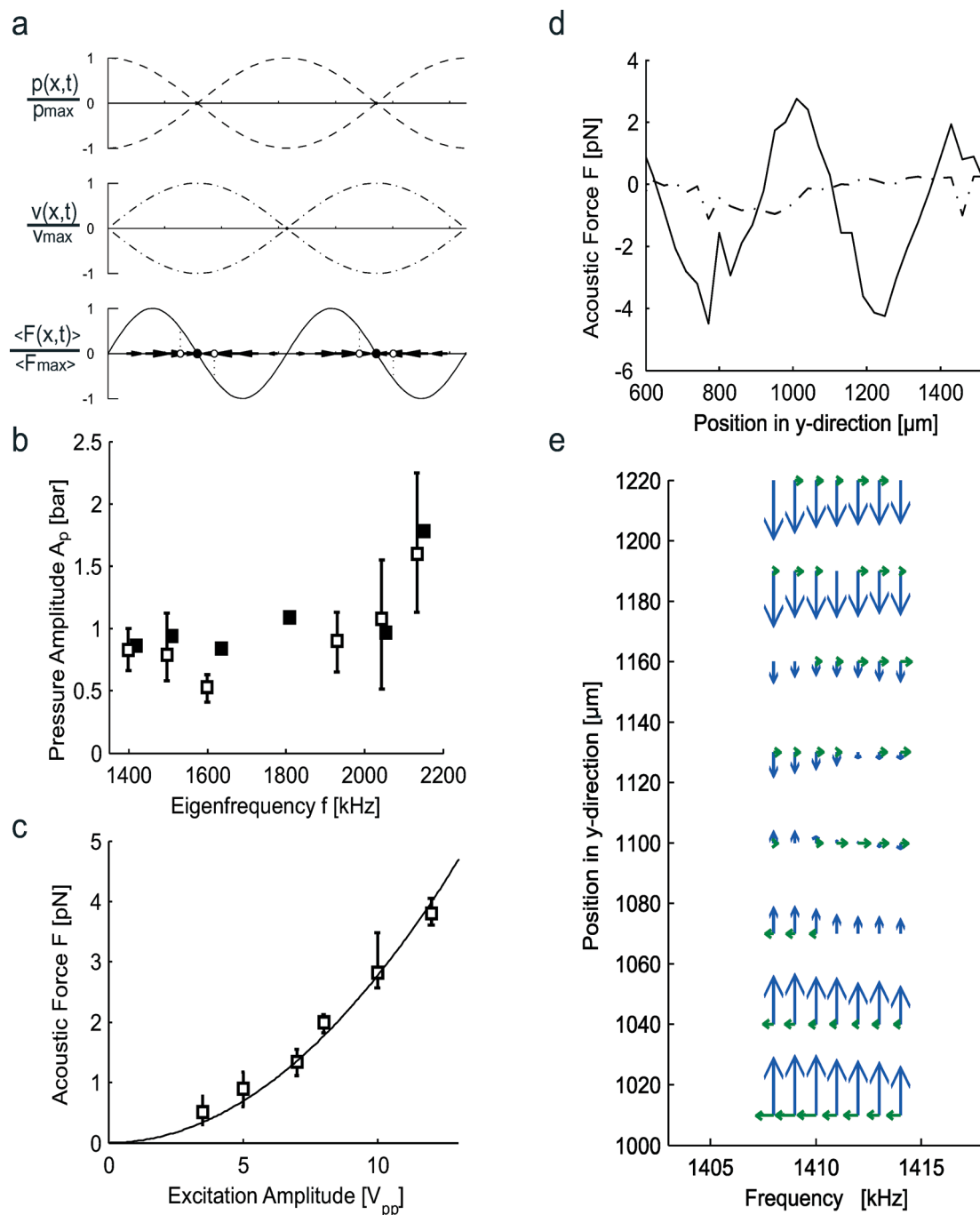
**Fig. 4** Pressure amplitude. a.) Schematic illustration of the normalized pressure, velocity, and force distribution for a 1D resonance mode. The pressure and velocity fields are shifted in phase by 90°, where the pressure shows its maximum at the solid–liquid interface for a sound-hard boundary condition. The force distribution has the double periodicity $\lambda_P = 2\lambda_F$ of the pressure distribution and the force arrows indicate the direction of force for a contrast factor $\Phi > 0$, leading to accumulation of particles at the position indicated by open circles, where the forces acting on the particle are at equilibrium. b.) Comparison of acoustic pressure amplitudes experimentally determined (open squares, all particle sizes) and numerically calculated (filled squares). Error bars indicate the absolute range of the experimental data as listed in Table 2. c.) The force on a 7.6 μm particle was determined using an increasing excitation amplitude (open squares, error bars indicate the absolute range of the determined force values from three different experiments). The data fit the theoretical equation nearly perfectly (solid line). d.) Force curve in the x- and y-direction detected by the bead displacement of a 7.6 μm particle at a 1411 kHz standing wave mode along the y-axis. e.) Vector plot of the force field generated from data as in Fig. 4d. The forces in the y-direction (BLUE) will lead to the particle motion towards the pressure nodes, whereas the forces in the x-direction (GREEN) are dominating at the pressure nodes of the standing wave field and lead in the experiment to particle concentration changes along the particle lines formed by the standing wave mode in the y-direction.

$A_F$ and subsequently the corresponding pressure amplitudes, which are again averaged to virtually identical values.

We believe that the reason for the offset in the experimentally determined forces is caused neither by the ultrasonic

**Table 1** Comparison of the collected experimental data for silica particles with 7.61 μm diameter and the numerical COMSOL simulations for different eigenfrequencies $f$. This data is graphically compared in Fig. 3d and 4b. The entries indicated with $|..|$ represent averaged values over all measurements and the index "COM" indicates the numerical results of the COMSOL Multiphysics simulation. The given $\lambda$ values belong to the sinusoidal force curve. The index "in" represents the values of single measurements. $|A_{F\ max}|$ is the average maximum force of all measurements. The entries signed with "x" are blank entries for the 10-line and 11-line modes that correspond to the missing experimental or numerical values, respectively

| Line mode | $|f|$ [kHz] | $f_{COM}$ [kHz] | $|\lambda_F|$ [μm] | $\lambda_{F\ COM}$ [μm] | $A_{F\ in}$ [pN] | $|A_{F\ max}|$ [pN] | $A_{F\ COM}$ [pN] | $|A_P|$ [bar] | $A_{P\ COM}$ [bar] |
|---|---|---|---|---|---|---|---|---|---|
| 7 | 1399 | 1420 | 542.5 | 571.4 | 3.90 | 2.97 | 3.13 | 0.83 | 0.86 |
|   |      |      |       |       | 3.55 |      |      |      |      |
|   |      |      |       |       | 1.45 |      |      |      |      |
| 8 | 1497 | 1510 | 510.0 | 500 | 4.95 | 4.16 | 6.52 | 0.79 | 0.94 |
|   |      |      |       |     | 3.64 |      |      |      |      |
|   |      |      |       |     | 3.88 |      |      |      |      |
| 9 | 1600 | 1636 | 453.8 | 444.4 | 2.80 | 1.97 | 4.12 | 0.53 | 0.84 |
|   |      |      |       |       | 1.30 |      |      |      |      |
|   |      |      |       |       | 1.80 |      |      |      |      |
| 10 | x | 1810 | x | 400 | x | x | 3.55 | x | 1.09 |
|    |   |      |   |     | x |   |      |   |      |
|    |   |      |   |     | x |   |      |   |      |
| 11 | 1930 | x | 372.5 | x | 7.12 | 5.94 | x | 0.9 | x |
|    |      |   |       |   | 4.47 |      |   |     |   |
|    |      |   |       |   | 6.22 |      |   |     |   |
| 12 | 2044 | 2055 | 335.0 | 333.3 | 12.33 | 10.33 | 9.95 | 1.07 | 0.97 |
|    |      |      |       |       | 9.94  |       |      |      |      |
|    |      |      |       |       | 8.71  |       |      |      |      |
| 13 | 2134 | 2152 | 310.1 | 307.7 | 12.77 | 13.87 | 20.2 | 1.6 | 1.78 |
|    |      |      |       |       | 6.51  |       |      |     |      |
|    |      |      |       |       | 22.34 |       |      |     |      |

field nor the optical trap: the zero position is determined by the references within each measurement, *i.e.*, when the acoustic field is switched off completely. An offset of a constant, unidirectional acoustical force $F_{offset}$ in one measurement varying from one measurement set to the next seems therefore highly unlikely. Similarly, an offset in the position determination due to misalignment in the optical trap is highly unlikely: first, the laser alignment was checked and seemed to be basically invariable. Assuming that small variations due to an asymmetrically focused beam would not be consistent in the determination of the trap center and would furthermore offset all signals within a measurement set by a given value, which is not the case. We rather see positive and negative offsets within all measurements. A possible source of the offset might be the determination of the bead position using image analysis and the reduction of the focus on the *y*-axis displacement, or alternatively, the effects of acoustic streaming, as described in the introduction. We, however, see the changes in focus and frequency-dependent rotation of imperfect dirty beads to be the most probable cause for slight offsets in the determination of the bead center, resulting in offset force values. It might be beneficial in the future to use the QPD position signal, which also allows for including the *z*-position signal to fully describe the movement of the bead within the acoustic regime.

So far, it is also impossible to directly predict the position of a pressure node, or, subsequently, the position of a zero force *a priori*, a useful piece of information to quickly access measurable properties in the small-range vicinity of a trapped/manipulated object. These positions are only determined *a posteriori* after time-consuming data analysis.

A method, which might possibly allow one to obtain this information, was recently described by ref. 25: it relies on an interference contrast method caused by the density differences in the solvent. However, this method so far requires large layers of solvents and, up till now, uses optical paths several orders of magnitude larger than the ones used for optical trapping.

## Quadratic dependency of the force amplitude on the excitation amplitude

An independent set of experiments was performed to confirm the quadratic dependency of the acoustic force in relation to an excitation amplitude change (Yosioka, eqn (2)). This was realized by applying a frequency sweep of 20 s from 1550 kHz to 1650 kHz at excitation amplitudes from 3.5 Vpp to 12 Vpp. The sweep ensured that the resonance near 1610 kHz was excited. Fig. 3c and Table 2 summarize the maximum force values resulting from the acoustic field. Force data were fit to a quadratic equation $f(x)$ of the form $f(x) = A_F x^2$ (Fig. 4c). The good agreement with the fit indicates that the acoustic force indeed scales with the square of the excitation amplitude, thus following eqn (2).

The results from the measurements that were used to determine the acoustic pressure at 5 Vpp are given in Fig. 4c and Table 2. We found the acoustic response of the system at 1610 kHz to fully agree with the existing theory and this allows one to generalize the linear pressure curve for all other modes in the acoustic system. It is thus possible to define the acoustic pressure *via* its excitation amplitude by taking one reference pressure at each eigenmode. This means that

**Table 2** Data of the excitation amplitude $A_{Ex}$ and dependent acoustic pressure amplitude $A_P$ for experiments with 7.61 μm silica particles. These data are partly shown in Fig. 4c. The values with index "1610" correspond to the 9-line mode at 1610 kHz. The entries indicated with |..| represent values averaged over all measurements. The "IN" column are the mV$_{pp}$ values of the sinusoidal input signal of the power amplifier generated by a frequency generator (Tektronix, AFG 3022B, Beaverton, OR, USA). The "OUT" column is the $V_{pp}$ values after the amplification (MKS Instrumente Deutschland GmbH, ENI 2100L RF, Bernhausen, Germany). The index "MAX" and "MIN" indicate the maximum and minimum values of the experimentally measured force and the calculated acoustic pressure amplitude

| $A_{Ex}$ IN [mV] | OUT [V] | $A_{F1610\ min}$ $A_{F1610\ max}$ [pN] | $|A_{F1610}|$ [pN] | $A_{P1610\ min}$ $A_{P1610\ max}$ [bar] | $|A_{P1610}|$ [bar] |
|---|---|---|---|---|---|
| 30 | 3.50 | 0.30 0.77 | 0.51 | 0.26 0.41 | 0.33 |
| 40 | 5 | 0.60 1.18 | 0.89 | 0.36 0.51 | 0.44 |
| 50 | 7 | 1.11 1.55 | 1.35 | 0.49 0.58 | 0.54 |
| 60 | 8 | 1.82 2.13 | 1.99 | 0.63 0.68 | 0.66 |
| 70 | 10 | 2.56 3.49 | 2.82 | 0.75 0.87 | 0.79 |
| 80 | 12 | 3.61 4.05 | 3.80 | 0.89 0.94 | 0.91 |

**Table 3** Pressure amplitude prediction based on data for different particle sizes. $A_{P\ min}$ and $A_{P\ max}$ define the measured minimum and maximum pressures obtained from the best possible sinusoidal fit of the force curve measured by optical trapping at an US frequency of 2044 kHz and an excitation amplitude of 5 Vpp. The entries indicated with |..| represent averaged values over all measurements

| Particle diameter [μm] | $|A_F|$ [pN] | $A_{P\ min}$ $A_{P\ max}$ [bar] | $|A_P|$ [bar] |
|---|---|---|---|
| 7.61 | 6.36 | 0.61 1.46 | 1.20 |
| 6.55 | 3.48 | 0.67 1.7 | 1.11 |
| 4.39 | 0.79 | 0.47 1.95 | 0.98 |

one single measurement at one single specific excitation amplitude throughout the whole frequency range is sufficient to predict the acoustic pressure amplitudes for all possible sets of parameters in our linear acoustic device.

### 2D Force field

The video detection provides the displacement data in the $x$- and $y$-direction along the channel. The data in the $y$-direction was used to find standing wave modes and for acoustic pressure amplitude prediction. Fig. 4d shows for the 1410 kHz mode that the forces in the $x$-direction are much smaller than those in the $y$-direction. Also, the force does not vary sinusoidally in the $x$-direction. The two curves in Fig. 4d are combined in a vector plot in Fig. 4e, where the shown vectors in the $y$-direction (blue) and in the $x$-direction (green) correlate with the particle motion in the trap due to this force

field. The particles will be moved toward the pressure nodes in the $y$-direction. The very small forces in the $x$-direction are not sufficient to organize the beads along the $x$-direction of the acoustic flow cell, as is evident from the continuous distribution of beads in Fig. 1c. Follow-up experiments with different flow cell geometries will be necessary to identify the source of this lateral force component and its potential applications.

## Conclusions

We have combined an US microfluidic cell with an optical trap to directly measure the 2D forces that act on a single bead in the acoustic field. Stationary and modulated acoustic standing waves are not only useful for the manipulation of particles or droplets, but also for living materials such as bacteria, individual cells or defined cell aggregates[1,26,27] A readily implementable low-cost method to simultaneously position and manipulate large numbers of particles is invaluable for high-throughput applications in biomedical analysis and research. For specific research fields, such as the mechano-transduction in cells, the added possibility to literally "tune-in" to the cell type, while holding the specimen in the focal plane can open up new experimental possibilities. For all such applications it is essential to be able to measure the forces that act on the samples, for which we have provided a direct method.

In principle, the measurements can be expanded to 3D by also measuring the forces along the $z$-axis. This can be realized by measuring the trap stiffness in the $z$-direction and by detecting the $z$-displacement of the bead out of the trap center. Although the bead displacement in the $z$-direction can also be measured by video analysis, a more accurate method would be to use the sum signal from the QPD.[28] As compared to the use of video analysis of the bead motion in 2D, which was used for our current work, the use of the QPD signal will eventually give an increased temporal resolution in all 3 dimensions. The sub-second time resolution will allow one to address so far inaccessible effects. Because the QPD detection also offers nanometer spatial resolution, the motion of smaller particles, particles trapped in very stiff optical traps or in more viscous solvents, becomes easier to detect as compared to that in video analysis. The challenge of using all the high-bandwidth information that is provided by the QPD lies in the large quantities of data, which in addition will have to be synchronized with the position of the bead in the microfluidic chamber. In future experiments, we plan to achieve this through a further automation of the measurement procedure. With a motorized sample stage, the trapped bead will be moved in a raster-like motion through the whole microfluidic chamber, while both the spatial coordinates and the power spectra of the trapped bead are recorded in 3D.

The reduction of the simulation to 2D instead of 3D is mainly due to the minimization of the calculation time. As a consequence, the loss of the third dimension leads to results independent of the $x$-direction and the device appeared

mechanically slightly stiffer. In the future, the numerical calculations should be expanded to the real 3D case.

## Acknowledgements

## References

1 B. Hammarstrom, M. Evander, H. Barbeau, M. Bruzelius, J. Larsson, T. Laurell and J. Nillsson, *Lab Chip*, 2010, **10**, 2251–2257.

2 J. Dual, P. Hahn, I. Leibacher, D. Moller and T. Schwarz, *Lab Chip*, 2012, **12**, 852–862.

3 D. Foresti, M. Nabavi, M. Klingauf, A. Ferrari and D. Poulikakos, *Proc. Natl. Acad. Sci. U. S. A.*, 2013, **110**, 12549–12554.

4 A. Lenshof, C. Magnusson and T. Laurell, *Lab Chip*, 2012, **12**, 1210–1223.

5 T. Laurell, F. Petersson and A. Nilsson, *Chem. Soc. Rev.*, 2007, **36**, 492–506.

6 P. Glynne-Jones and M. Hill, *Lab Chip*, 2013, **13**, 1003–1010.

7 R. Barnkob, P. Augustsson, T. Laurell and H. Bruus, *Lab Chip*, 2010, **10**, 563–570.

8 G. Thalhammer, R. Steiger, M. Meinschad, M. Hill, S. Bernet and M. Ritsch-Marte, *Biomed. Opt. Express*, 2011, **2**, 2859–2870.

9 A. Ashkin, *Phys. Rev. Lett.*, 1970, **24**, 156–159.

10 A. Ashkin, K. Schutze, J. M. Dziedzic, U. Euteneuer and M. Schliwa, *Nature*, 1990, **348**, 346–348.

11 P. G. Bassindale, D. B. Phillips, A. C. Barnes and B. W. Drinkwater, *Appl. Phys. Lett.*, 2014, **104**, 163504.

12 A. Ashkin, J. M. Dziedzic, J. E. Bjorkholm and S. Chu, *Opt. Lett.*, 1986, **11**, 288.

13 K. Bodensiek, W. X. Li, P. Sanchez, S. Nawaz and I. A. T. Schaap, *Rev. Sci. Instrum.*, 2013, **84**, 113707.

14 F. Gittes and C. F. Schmidt, *Methods Cell Biol.*, 1998, **55**, 129–156.

15 K. Svoboda and S. M. Block, *Annu. Rev. Biophys. Biomol. Struct.*, 1994, **23**, 247–285.

16 K. C. Vermeulen, G. J. L. Wuite, G. J. M. Stienen and C. F. Schmidt, *Appl. Opt.*, 2006, **45**, 1812–1819.

17 L. V. King, *Proc. R. Soc. London, Ser. A*, 1934, **147**, 212–240.

18 K. Yosioka and Y. Kawasima, *Acustica*, 1955, **5**, 167–173.

19 L. P. Gor'kov, *Sov. Phys. Dokl.*, 1962, **6**, 773–775.

20 W. L. Nyborg, *J. Acoust. Soc. Am.*, 1958, **30**, 329–339.

21 J. M. Andres and U. Ingard, *J. Acoust. Soc. Am.*, 1953, **25**, 932–938.

22 H. Bruus, *Lab Chip*, 2011, **11**, 3742–3751.

23 H. Bruus, *Lab Chip*, 2012, **12**, 20–28.

24 S. Nawaz, P. Sanchez, K. Bodensiek, S. Li, M. Simons and I. A. Schaap, *PLoS One*, 2012, **7**, e45297.

25 D. Moller, N. Degen and J. Dual, *J. Nanobiotechnol.*, 2013, **11**, 21.

26 A. Neild, S. Oberti, G. Radziwill and J. Dual, *Biotechnol. Bioeng.*, 2007, **97**, 1335–1339.

27 M. A. H. Weiser, R. E. Apfel and E. A. Neppiras, *Acustica*, 1984, **56**, 114–119.

28 J. K. Dreyer, K. Berg-Sorensen and L. Oddershede, *Appl. Opt.*, 2004, **43**, 1991–1995.

29 R. Barnkob, P. Augustsson, T. Laurell and H. Bruus, *Phys. Rev. E*, 2012, **86**, 056307.